Opposing Effects of Cucurbit[7]uril and 1,2,3,4,6-penta-O-galloyl-β-D-glucopyranose on Amyloid $\beta_{25\text{-}35}$ Assembly

Natália E. C. de Almeida,[†] Thanh D. Do, [†,¥] Michael Tro,[†] Nichole E. LaPointe,[‡] Stuart C. Feinstein,[‡] Joan-Emma Shea,[†] Michael T. Bowers[†,*]

[†] Department of Chemistry and Biochemistry, [‡] Neuroscience Research Institute and Department of Molecular Cellular and Developmental Biology, University of California, Santa Barbara, California 93106, United States.

*Corresponding author: Michael T. Bowers.

Tel: +1-805-893-2673; E-mail address: bowers@chem.ucsb.edu

SUPPPORTING INFORMATION

This material is available free of charge via the Internet at http://pubs.acs.org

S1. Materials and Methods

S1.1. Materials and Sample preparation

Peptide and sample preparation for IMS-MS and TEM experiments

A$\beta_{25\text{-}35}$ peptide (GSNKGAIIGLM) with free termini was purchased from rPeptide (Bogard, GA). The peptide solution was prepared in submicron filtered water (HPLC grade) acidified with formic acid (0.1% (v/v)) purchased from Fisher Scientific (Bridgewater, NJ) (final peptide concentration 100 µM). 1,2,3,4,6-penta-O-galloyl-β-D-glucopyranose (PGG) was purchased from Sigma-Aldrich (St. Louis, MO, USA) and dissolved in water containing 20% (v/v) methanol purchased from TCI America (Portland, OR, USA), whereas cucurbit[7]uril (CB[7]) was purchased from Sigma-Aldrich (St. Louis, MO, USA) and dissolved in water acidified with formic acid (0.1% (v/v)).

The A$\beta_{25\text{-}35}$ was incubated with the ligands at molar ratios of 1:1 and 1:10. A positive control was performed using an A$\beta_{25\text{-}35}$ solution without the ligands and, after 1 week of incubation time at room temperature, the samples were analyzed by ion mobility spectrometry coupled mass spectrometry (IMS-MS) and by transmission electron microscopy (TEM). For the TEM analysis, samples were adsorbed onto 300 mesh formvar/carbon copper grids (Electron Microscopy Sciences) for 1.5 min. Grids were subsequently rinsed with deionized water and then stained for 1 min with 2% uranyl acetate. Additionally, CB[7] was added to a A$\beta_{25\text{-}35}$ solution previously incubated for one week with PGG (at 1:1 ratio) to the final A$\beta_{25\text{-}35}$:PGG:CB[7] molar ratio of 1:1:5 and 1:1:10, and then incubated an additional two days prior to TEM analysis.

S1.2. Methods

S.1.2.1. Ion mobility spectrometry coupled mass spectrometry (IMS-MS).

The samples were analyzed on a home built ion mobility spectrometer coupled to a mass spectrometer (IMS-MS) comprised of a nano-electrospray ionization (nano-ESI) source, an ion funnel, a temperature-controlled drift cell, a quadrupole mass filter and an electron multiplier detector.[1,2] Briefly, gold coated borosilicate capillaries made on an in-house micropipette puller (Sutter Instrument Co., Novato, CA) were used to load the samples. A positive voltage was applied and ions were continuously formed, focused and stored in the ion funnel. A 10 μs pulse of ions was injected into a temperature-controlled drift cell filled with ~5 Torr of helium gas where they gently passed through under the influence of a weak electric field (5-20 V cm^{-1}). The injection energy may be varied from ~20 to ~150 eV but was normally kept as ~40 eV to minimize thermal heating of the ions and allow accurate mobility measurements. The ions leaving the drift cell were mass analyzed using a quadrupole mass filter, detected by a conversion dynode/electron multiplier arrangement, and recorded as a function of their arrival time to obtain arrival time distributions (ATDs).

The injected ions in the drift cell experience a constant force from the electric field, *E*, that is balanced by a retarding frictional force due to collisions with the buffer gas. As a result, the velocity (v_d) of the ions in the buffer gas is constant and proportional to the electric field, equation 1;[3]

$$\vec{v}_d = K\vec{E} \tag{1}$$

where *K* is the mobility. The mobility of the ion packet is dependent on the temperature (*T*) and the pressure (*P*) of the buffer gas; hence the standard state reduced mobility (K_0) is more convenient to use:

$$K_0 = K \cdot \frac{P}{760\ \text{Torr}} \cdot \frac{273.16\text{K}}{T} \tag{2}$$

The ions leaving the drift cell are mass analyzed and detected as a function of arrival time, and the reduced mobility can be obtained[4] from the instrument parameters by converting equation 1 to equation 3 and by plotting t_A versus P/V;

$$t_A = \frac{l^2}{K_0} \cdot \frac{273.16\text{K}}{760\ \text{Torr} \cdot T} \cdot \frac{P}{V} + t_0 \tag{3}$$

where l is the length of the drift cell (4.503 cm), P denotes the gas pressure (in Torr), V is the voltage across the cell and t_0 the time the ions spend outside the drift cell before hitting the detector. From the kinetic theory of gases,[3] K_0 can be related to the collision cross section σ by equation 4:

$$K_0 = \frac{3q}{16N} \cdot \left[\frac{2\pi}{\mu k_b T}\right]^{1/2} \cdot \frac{1}{\sigma} \tag{4}$$

Here, N is the buffer gas number density at STP, q is the ion charge, μ is the reduced mass of the ion/helium collision system and k_b is the Boltzmann constant. The flux of ions exiting the drift tube can be calculated using ion transport theory. By assuming that the ion packet is taken as a periodic delta function, the flux is given by equation 5.[3,4]

$$\phi(0,z,t) = \frac{s \cdot a \cdot e^{-\alpha t}}{4(\pi D_L t)^{1/2}} \cdot \left[v_d + \frac{z}{t}\right] \cdot \left[1 - e^{\left(-r_0^2/4D_T t\right)}\right] \cdot e^{\left(-(z-v_d t)^2/4D_L t\right)} \tag{5}$$

where z denotes the distance of the ion traveled, a is the area of the exit aperture, r_0 is the radius of the initial ion packet, s is the initial ion density, α is the loss of ions due to reactions in the drift tube, and D_L and D_T refer to the longitudinal and transverse diffusion coefficients, respectively. This equation allows the calculation of the arrival time peak shape expected for a pulse of ions with a single collision cross section.

As a result, multiple features may appear in the same ATD, indicating the presence of different oligomers with the same m/z but distinct n/z or distinct conformations of the same oligomer. Extended conformers experience more collisions with the buffer gas than compact ones, leading to longer arrival times and larger cross sections. For oligomers

with the same *n*/*z*, the larger oligomers would transverse the drift cell faster as they possess a higher charge per unit cross section (for example, the *n*/*z* = 2/2 dimer has twice the charge of the *n*/*z* = 1/1 monomer but it is not twice as large due to the contact surface between the two monomers in the dimer. Hence dimers arrive before monomer, trimers before dimers etc. at the same *n*/*z*).

S.1.2.2. Transmission electron microscopy (TEM)

TEM images were taken using a JEOL 123 microscope, an ORCA camera, and AMT Image Capture Software v. 5.24.

S.1.2.3. Explicit solvent molecular dynamics simulations

Force field parameterization. The three-dimensional structure of CB[7] was obtained from the X-ray crystal structure solved by Kim, J. et al.[5] Solvent ions were removed. The three-dimensional structure of PGG was built and geometry optimized using the Avogadro molecular editor (http://avogadro.cc).[6] The bare ligand molecule was subjected to geometry optimization and partial charge fitting using the RESP ESP charge Derive Server (http://q4md-forcefieldtools.org/REDServer/).[7-10] We used the RESP-A1A charge model (i.e., HF level and 6-31G* basis set; Connolly surface algorithm used in MEP computation and two stage RESP fit with qwt=0.0005/0.001) to be compatible with the Amber force fields. Additional parameters for PGG were chosen from the GAFF force field.[11,12]

Simulation details. The A$\beta_{25\text{-}35}$ monomer was built using the *tleap* module available from the Amber12 package.[11] The force field parameters of this peptide are from the Amber ff12SB. Each simulation contains four A$\beta_{25\text{-}35}$ monomers and four ligands (PGG or CB[7]). The initial positions of each peptide and ligand were set by VMD.[13] Four Cl- ions were added to neutralize the net charge. The whole system was solvated in an

octahedral TIP3P water box using the spacing distance of 11 Å around the molecules, so that there were approximately 8,000 water molecules. The solvated systems were subjected to a series of short minimization and heating cycles to equilibrate the solvent at 300K. The MD simulation was performed in the NPT ensemble using the periodic boundary condition and a time step of 2 fs. Temperature was regulated by Langevin dynamics with a collision frequency of 1.0. The MD trajectory was 180-ns long for each system.

S2. Mass spectra

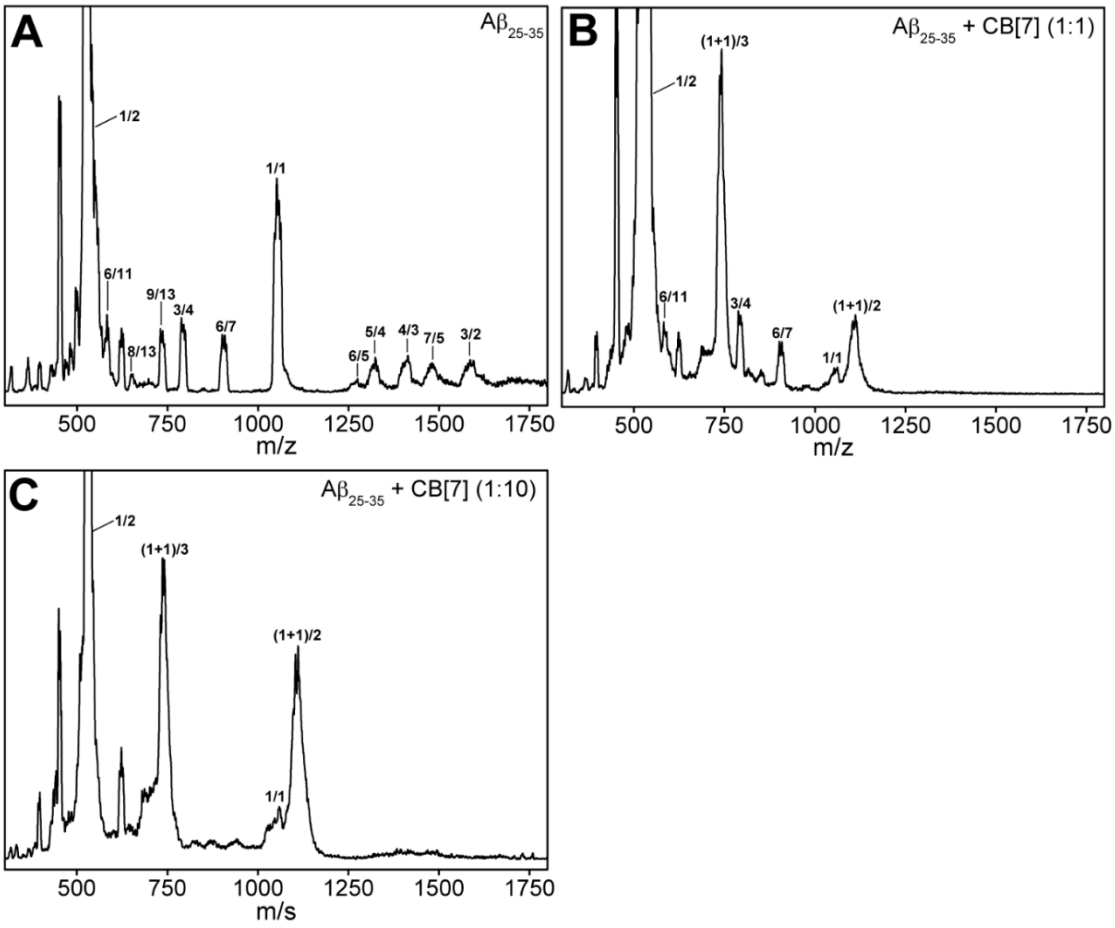

Figure S1. ESI-Q spectra of A$\beta_{25\text{-}35}$ incubated (A) in water acidified with formic acid (0.1% v/v), (B) with CB[7] at 1:1 and (C) at 1:10 A$\beta_{25\text{-}35}$:CB[7] mixtures. The A$\beta_{25\text{-}35}$ mass spectrum (Fig. A) displays two major peaks at *m*/*z* 530 (*n*/*z* 1/2) and *m*/*z* 1060 (*n*/*z* 1/1 and 2/2), and minor peaks at *m*/*z* 578 (*n*/*z* 6/11), *m*/*z* 652 (*n*/*z* 8/13), *m*/*z* 733 (*n*/*z* 9/13), *m*/*z* 795 (*n*/*z* 3/4), *m*/*z* 908 (*n*/*z* 6/7), *m*/*z* 1272 (*n*/*z* 6/5), *m*/*z* 1325 (*n*/*z* 5/4), *m*/*z* 1413 (*n*/*z* 4/3), *m*/*z* 1484 (*n*/*z* 7/5) and *m*/*z* 1590 (*n*/*z* 3/2). From the mass spectrum obtained for the A$\beta_{25\text{-}35}$:CB[7] mixture at a ratio of 1 to 1 (Fig. B), the two most abundant peaks at *m*/*z* 741 (*n*/*z* (1+1)/3) and 1111 (*n*/*z* (1+1)/2 and (2+2)/4) are attributed to A$\beta_{25\text{-}35}$:CB[7] complexes, which refer to the monomer and the dimer bound to one and two CB[7] molecules, respectively. The remaining A$\beta_{25\text{-}35}$ homo-oligomers are the monomers at *m*/*z* 530 (*n*/*z* 1/2) and *m*/*z* 1060 (*n*/*z* 1/1), the dimer at *m*/*z* 1060 (*n*/*z* 2/2), the trimer at *m*/*z* 795 (*n*/*z* 3/4) and the hexamers at *m*/*z* 908 (*n*/*z* 6/7) and *m*/*z* 578 (*n*/*z* 6/11). At A$\beta_{25\text{-}35}$:CB[7] 1:10 ratio

(Fig. C), the large A$\beta_{25\text{-}35}$ homo-oligomers fully deplete, whereas the population increases for the peaks at *m*/*z* 741 and 1111 that correspond to the A$\beta_{25\text{-}35}$:CB[7] complexes.

S3. Ion mobility data and Arrival Time Distributions (ATDs)

S3.1. ATDs for A$\beta_{25\text{-}35}$

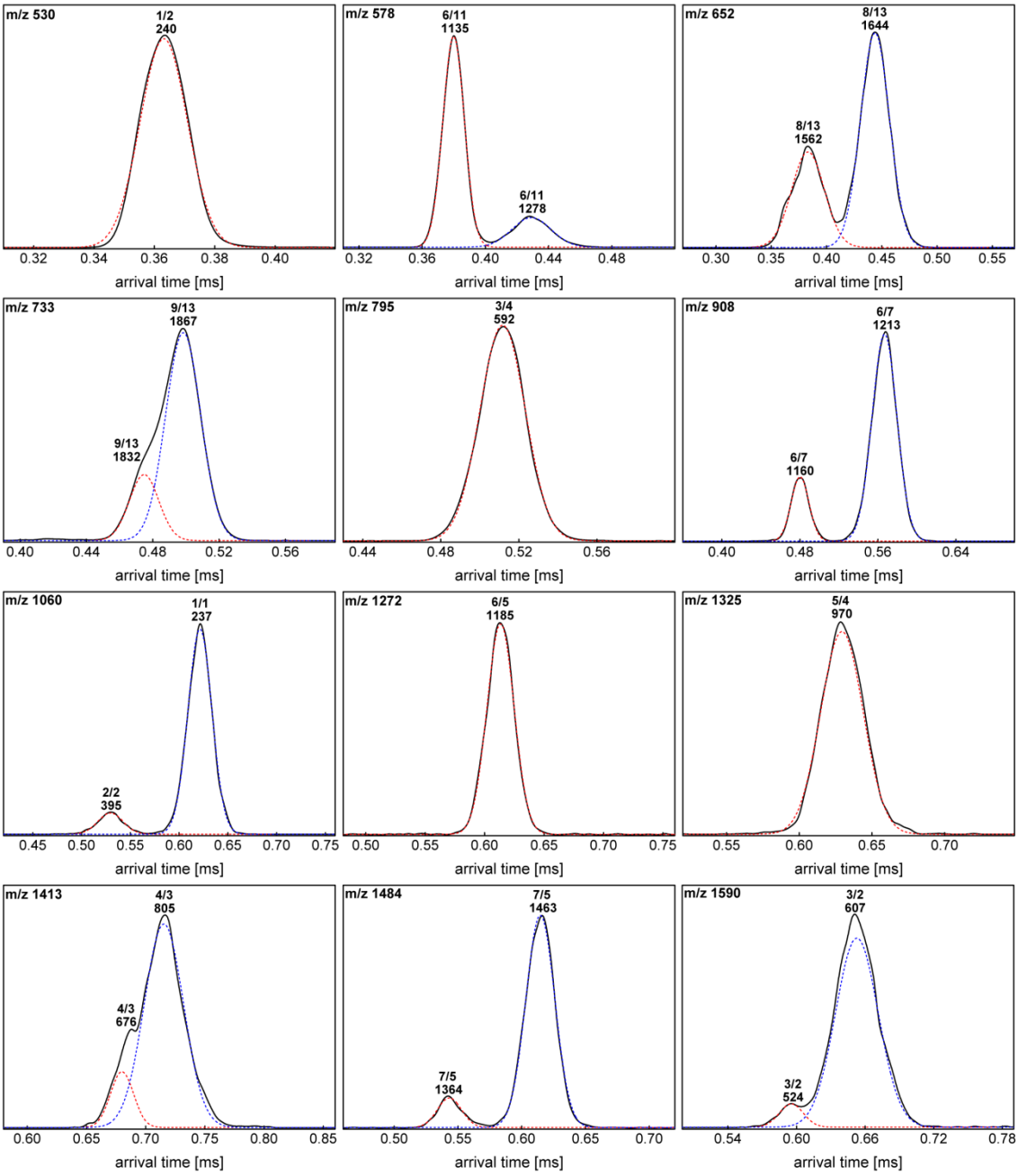

Figure S2. ATDs of A$\beta_{25\text{-}35}$ (100 µM). The peak at *m*/*z* 530 was the most abundant, which refers to a single monomer species with a collision cross section of 240 Å^2. It is consistent with the compact monomer cross section (237 Å^2) obtained from the *m*/*z* 1060 ATD, which also contains a dimer (395 Å^2). Other abundant peaks are *m*/*z* 908 (hexamers, 1160 and 1213 Å), 795 (trimer, 592 Å), 733 (nonamers, 1832 and 1867 Å) and 578 (hexamers, 1135 and 1278 Å), which display

larger and extended oligomers. The minor peaks at *m*/*z* 652, 1272, 1325, 1413, 1484 and 1590 refer to octamers (1562 and 1644 Å), hexamer (1185 Å), pentamer (970 Å), tetramers (676 and 805 Å), heptamers (1364 and 1463 Å) and trimers (524 and 607 Å), respectively.

Table S1. Collision cross section for homo-oligomers of A$\beta_{25\text{-}35}$.

m/z	n A$\beta_{25\text{-}35}$	z charge	Experimental Cross Section[a], σ_{exp}	Idealized growth model Isotropic[b], $\sigma_{iso}(n)$
530	1	2	240	237
578	6	11	1135	782
578	6	11	1278	782
652	8	13	1562	948
652	8	13	1644	948
733	9	13	1832	1025
733	9	13	1867	1025
795	3	4	592	493
908	6	7	1160	782
908	6	7	1213	782
1060	1	1	237	237
1060	2	2	395	376
1272	6	5	1185	782
1325	5	4	970	693
1413	4	3	676	597
1413	4	3	805	597
1484	7	5	1364	867
1484	7	5	1463	867
1590	3	2	524	493
1590	3	2	607	493

[a] values in Å^2

[b] given by $\sigma_{iso}(n) = \sigma_{A\beta_{25\text{-}35,mon}} \cdot n^{2/3}$

S3.2. ATDs for A$\beta_{25\text{-}35}$ incubated with CB[7]

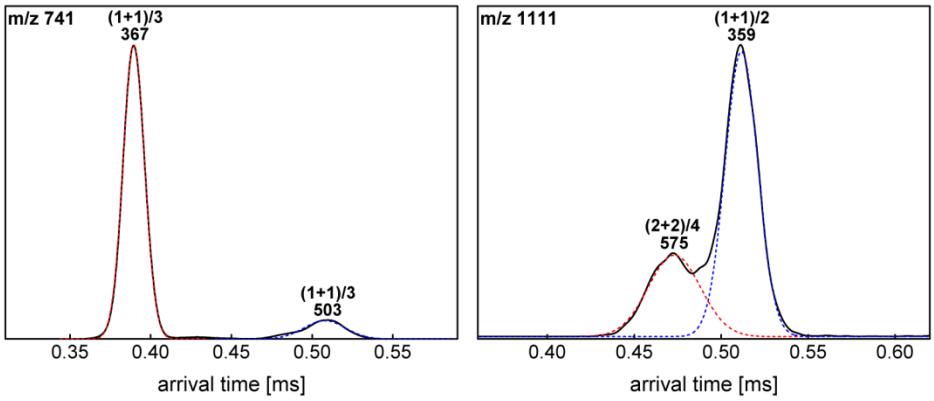

Figure S3. ATDs of A$\beta_{25\text{-}35}$ (100 µM) incubated with CB[7] at the molar ratio of 1:1. The data show ATDs for A$\beta_{25\text{-}35}$ monomer and dimer bound to one and two CB[7] molecules. The peak at *m*/*z* 741 displays a compact monomer bound to one CB[7] molecule (*n*/*z* (1+1)/3) with cross section of 367 Å, and it also contains a smaller feature which consists of an extended monomer with cross section of 503 Å. Monomer and dimer complexes with one and two CB[7] molecules are also detected at *m*/*z* 1111 (*n*/*z* (1+1)/2 and (2+2)/4), for which the cross sections were 359 and 575 Å, respectively.

Table S2. Collision cross section for hetero-oligomers of A$\beta_{25\text{-}35}$ incubated with CB[7] at the molar ratio of 1:1.

m/z	n A$\beta_{25\text{-}35}$	k CB[7]	z charge	Cross section[a] σ_{exp}	Isotropic model[a,b] σ_{iso}	Ratio experimente/ isotropic[c] $\mathcal{E}(n,k)$	Isotropic A$\beta_{25\text{-}35}$[d] $\sigma_{iso}(n)$	Corrected A$\beta_{25\text{-}35}$[a,e] $\sigma_{corr}(n,k)$
741	1	1	3	367	360	1.018149	237	241
741	1	1	3	503	360	1.395446	237	331
1111	1	1	2	359	360	0.995955	237	236
1111	2	2	4	575	572	1.004908	376	378

[a] values in Å^2.

[b] isotropic cross section is calculated as $\sigma_{iso}(n,k) = [n \cdot \sigma_{A\beta_{25\text{-}35,mon}}{}^{3/2} + k \cdot \sigma_{CB[7],mon}{}^{3/2}]^{2/3}$, where n and k are the number of A$\beta_{25\text{-}35}$ and the number of CB[7] molecules, respectively, and $\sigma_{A\beta_{25\text{-}35,mon}}$ (237 Å^2) and $\sigma_{CB[7],mon}$ (217 Å^2) are the collision cross sections of the compact monomers of A$\beta_{25\text{-}35}$ and cucurbit[7]uril (CB[7]), respectively. The value of 217 Å^2 for the collision cross section of CB[7] was obtained from calculating the cross section of the X-ray structure of CB[7] (see Kim, J. et al[5]) using the trajectory (TJ)[14,15] and projected superposition approximation (PSA)[16,17] methods.

[c] given by $\mathcal{E}(n,k) = \sigma_{exp} / \sigma_{iso}(n,k)$.

[d] given by $\sigma_{iso}(n) = \sigma_{A\beta_{25\text{-}35,mon}} \cdot n^{2/3}$.

[e] given by $\sigma_{corr}(n,k) = \sigma_{iso}(n) \cdot \mathcal{E}(n,k) = \sigma_{iso}(n) \cdot [\sigma_{exp} / \sigma_{iso}(n,k)]$.

S3.3. ATDs for A$\beta_{25\text{-}35}$ incubated with PGG

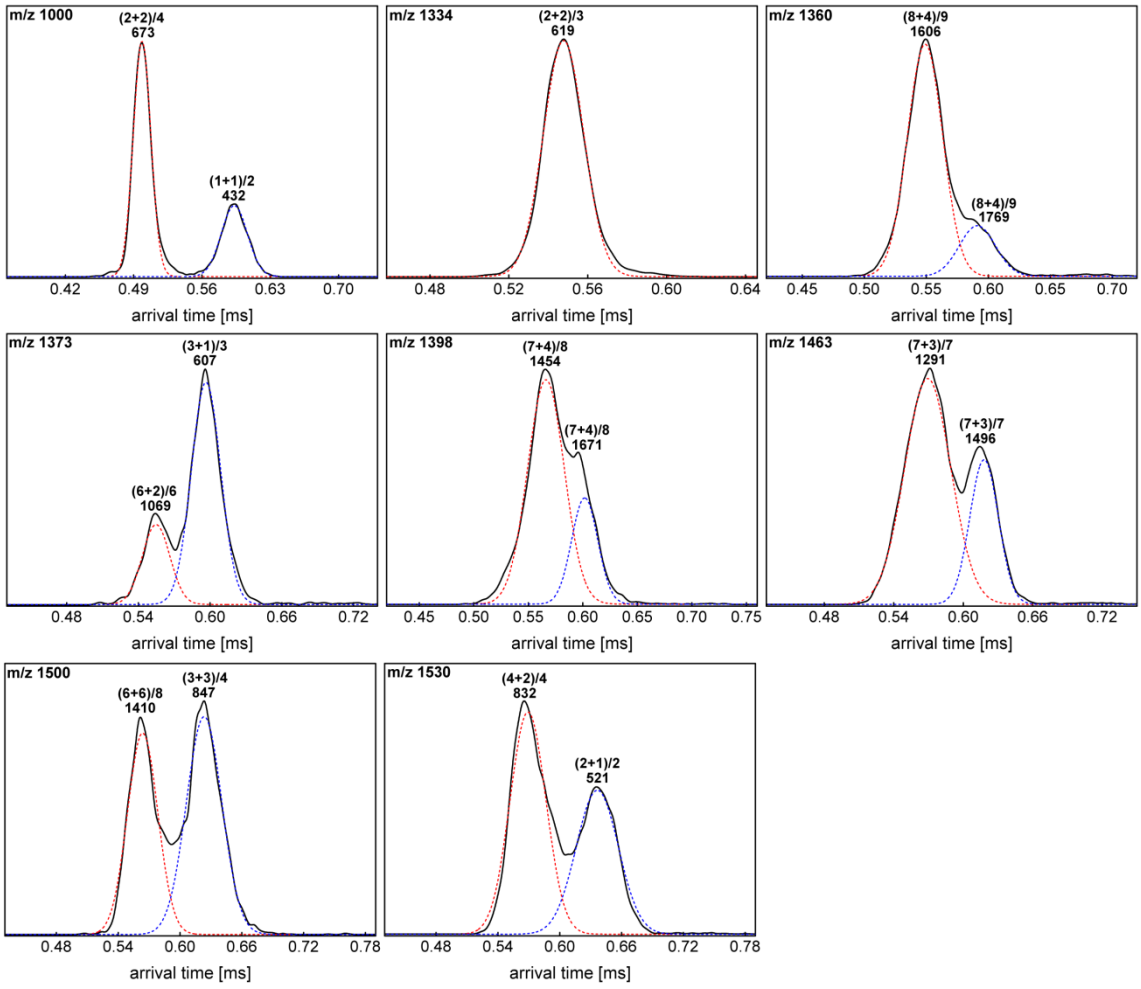

Figure S4. ATDs of A$\beta_{25\text{-}35}$ (100 µM) incubated with PGG at the molar ratio of 1:1. From the data, different complexes of A$\beta_{25\text{-}35}$ with PGG were observed, which correspond to A$\beta_{25\text{-}35}$ monomer, dimer, trimer, tetramer, hexamer, heptamer and octamer bound to several PGG molecules. The ATD of *m*/*z* 1000 displays an A$\beta_{25\text{-}35}$ monomer and a dimer bound to one and two PGG molecules (*n*/*z* (1+1)/2 and (2+2)/4) with cross sections of 432 and 673 Å, respectively. Similarly, dimers with two and one PGG molecules are found at *m*/*z* 1334 (*n*/*z* (2+2)/3, 619 Å) and at *m*/*z* 1530 (*n*/*z* (2+1)/2, 521 Å), which also shows a tetramer bound to two ligand molecules (*n*/*z* (4+2)/4, 832 Å). Trimer complexes containing one and three PGG molecules are observed at *m*/*z* 1373 (*n*/*z* (3+1)/3, 607 Å) and at *m*/*z* 1500 (*n*/*z* (3+3)/4, 847 Å), which also display oligomeric A$\beta_{25\text{-}35}$ hexamers bound to two and six PGG molecules (*n*/*z* (6+2)/6, 1069 Å; *n*/*z* (6+6)/8, 1410 Å). A$\beta_{25\text{-}35}$ heptamers bound to four and three PGG molecules are found at *m*/*z* 1398 (*n*/*z* (7+4)/8,

1454 and 1671 Å) and at *m*/*z* 1463 (*n*/*z* (7+3)/7, 1291 and 1496 Å). Finally, octamer complexes containing four bound PGG molecules are observed at *m*/*z* 1360 (*n*/*z* (8+4)/9) with cross sections of 1606 and 1769 Å.

Table S3. Collision cross section for hetero-oligomers of A$\beta_{25\text{-}35}$ incubated with PGG at the molar ratio of 1:1.

m/z	n A$\beta_{25\text{-}35}$	p PGG	z charge	Cross section[a] σ_{exp}	Isotropic model[a,b] σ_{iso}	Ratio experimente/ isotropic[c] $\mathcal{E}(n,p)$	Isotropic A$\beta_{25\text{-}35}$[d] $\sigma_{iso}(n)$	Corrected A$\beta_{25\text{-}35}$[a,e] $\sigma_{corr}(n,p)$
1000	1	1	2	432	363	1.189928	237	282
1000	2	2	4	673	576	1.167792	376	439
1334	2	2	3	619	576	1.074091	376	404
1360	8	4	9	1606	1213	1.323761	948	1255
1360	8	4	9	1769	1213	1.458115	948	1382
1373	3	1	3	607	587	1.034584	493	510
1373	6	2	6	1069	931	1.147804	782	898
1398	7	4	8	1454	1142	1.272801	867	1104
1398	7	4	8	1671	1142	1.462758	867	1268
1463	7	3	7	1291	1077	1.198803	867	1039
1463	7	3	7	1496	1077	1.389163	867	1204
1500	3	3	4	847	755	1.121604	493	553
1500	6	6	8	1410	1199	1.176220	782	920
1530	2	1	2	521	481	1.082119	376	407
1530	4	2	4	832	764	1.088614	597	650

[a] values in Å^2.

[b] isotropic cross section is calculated as $\sigma_{iso}(n,p) = [n \cdot \sigma_{A\beta_{25\text{-}35,mon}}{}^{3/2} + p \cdot \sigma_{PGG,mon}{}^{3/2}]^{2/3}$, where n and p are the number of A$\beta_{25\text{-}35}$ and PGG molecules, respectively, and $\sigma_{A\beta_{25\text{-}35,mon}}$ (237 Å^2) and $\sigma_{PGG,mon}$ (220 Å^2) are the collision cross sections of the compact monomers of A$\beta_{25\text{-}35}$ and 1,2,3,4,6-penta-O-galloyl-β-D-glucopyranose (PGG), respectively. The value of 220 Å^2 for the collision cross section of PGG was obtained from averaging the cross sections of geometry-optimized PGG obtained from the TJ[14,15] and PSA[16,17] methods.

[c] given by $\mathcal{E}(n,p) = \sigma_{exp} / \sigma_{iso}(n,p)$.

[d] given by $\sigma_{iso}(n) = \sigma_{A\beta_{25\text{-}35,mon}} \cdot n^{2/3}$.

[e] given by $\sigma_{corr}(n,p) = \sigma_{iso}(n) \cdot \mathcal{E}(n,p) = \sigma_{iso}(n) \cdot [\sigma_{exp} / \sigma_{iso}(n,p)]$.

S3.4. ATDs for A$\beta_{25\text{-}35}$ incubated with PGG and CB[7]

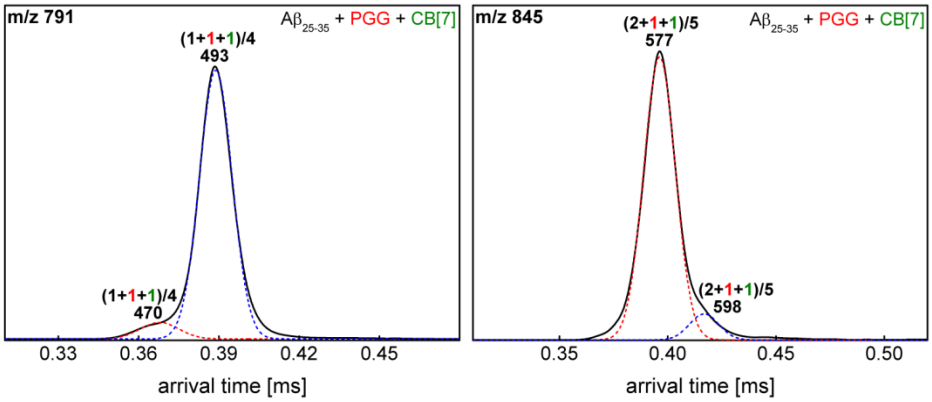

Figure S5. ATDs of A$\beta_{25\text{-}35}$ (100 µM) incubated with PGG and CB[7] at the molar ratio of 1:1:1. The ATDs are for A$\beta_{25\text{-}35}$ monomer and dimer bound to one PGG and to one CB[7] molecule. The ATD at *m*/*z* 791 shows two monomers bound to one PGG and to one CB[7] molecule (*n*/*z* (1+1+1)/4) with cross sections of 470 and 493 Å. The dimer complexes with one bound molecule of PGG and CB[7] are found at *m*/*z* 845 (*n*/*z* (2+1+1)/5), for which the cross sections were 577 and 598 Å, respectively.

Table S4. Collision cross section for hetero-oligomers of A$\beta_{25\text{-}35}$ incubated with PGG and CB[7] at the molar ratio of 1:1:1.

m/z	n A$\beta_{25\text{-}35}$	p PGG	k CB[7]	z charge	Cross section[a] σ_{exp}	Isotropic model[a,b] σ_{iso}	Ratio experimente/ isotropic[c] $\mathcal{E}(n,p,k)$	Isotropic A$\beta_{25\text{-}35}$[d] $\sigma_{iso}(n)$	Corrected A$\beta_{25\text{-}35}$[a,e] $\sigma_{corr}(n,p,k)$
791	1	1	1	4	470	468	1.004959	237	238
791	1	1	1	4	493	468	1.054138	237	250
845	2	1	1	5	577	574	1.004792	376	378
845	2	1	1	5	598	574	1.041361	376	392

[a] values in Å^2.

[b] isotropic cross section is calculated as $\sigma_{iso}(n,p,k) = [n \cdot \sigma_{A\beta_{25\text{-}35,mon}}{}^{3/2} + p \cdot \sigma_{PGG,mon}{}^{3/2} + k \cdot \sigma_{CB[7],mon}{}^{3/2}]^{2/3}$, where n, p and k are the number of A$\beta_{25\text{-}35}$, PGG and CB[7] molecules, respectively, and $\sigma_{A\beta_{25\text{-}35,mon}}$ (237 Å^2), $\sigma_{PGG,mon}$ (220 Å^2) and $\sigma_{CB[7],mon}$ (217 Å^2) are the collision cross sections of the compact monomers of A$\beta_{25\text{-}35}$, 1,2,3,4,6-penta-O-galloyl-β-D-glucopyranose (PGG) and cucurbit[7]uril (CB[7]), respectively. The values of 220 and 217 Å^2 for the collision cross section of PGG and CB[7] were obtained from theory, as described before.

[c] given by $\mathcal{E}(n,p,k) = \sigma_{exp} / \sigma_{iso}(n,p,k)$.

[d] given by $\sigma_{iso}(n) = \sigma_{A\beta_{25\text{-}35,mon}} \cdot n^{2/3}$.

[e] given by $\sigma_{corr}(n,p,k) = \sigma_{iso}(n) \cdot \mathcal{E}(n,p,k) = \sigma_{iso}(n) \cdot [\sigma_{exp} / \sigma_{iso}(n,p,k)]$.

S4. Transmission electron microscopy (TEM) data of A$\beta_{25\text{-}35}$ incubated with PGG followed by CB[7]

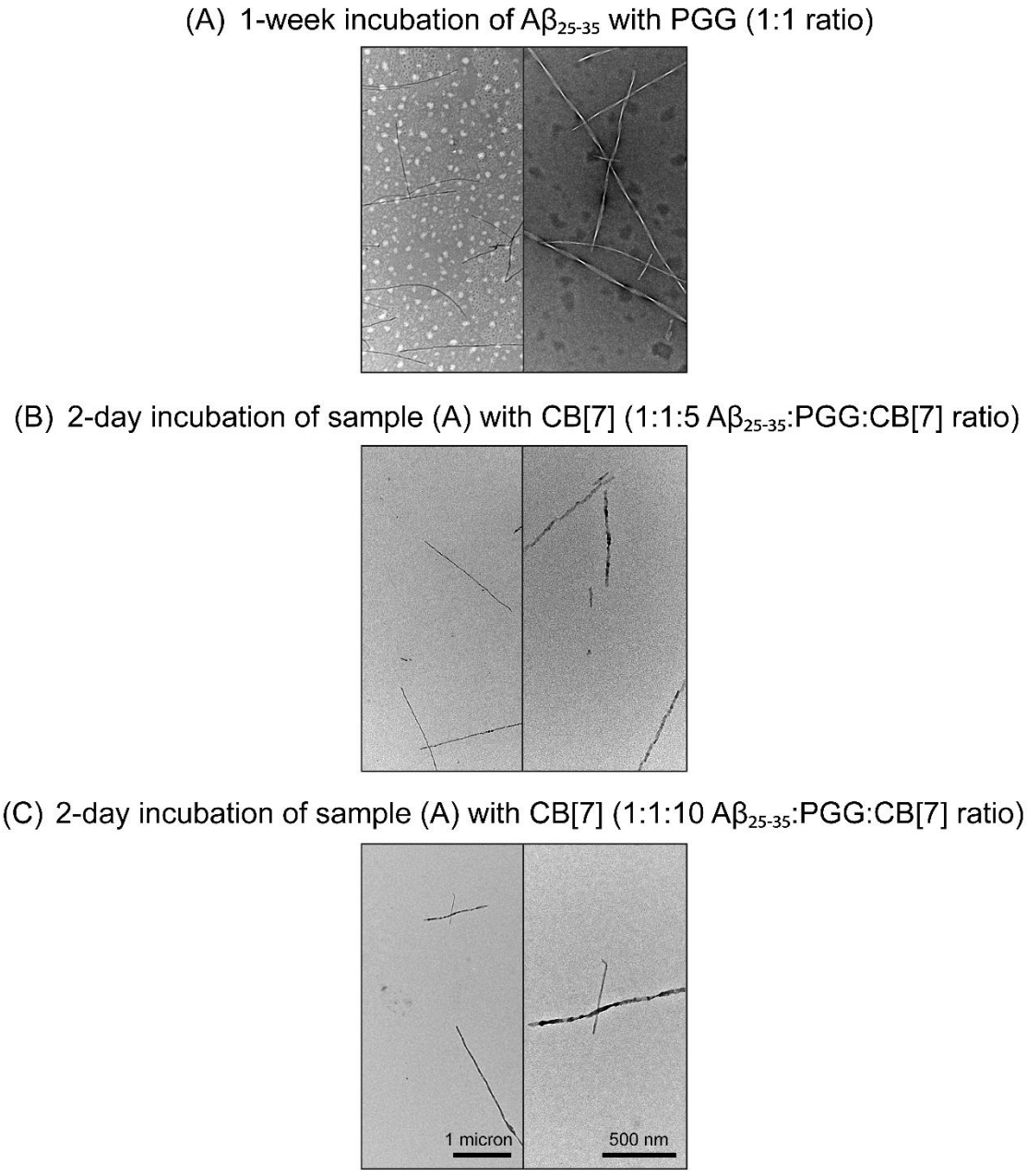

Figure S6. TEM images for recovery experiments. (A) A$\beta_{25\text{-}35}$ solution incubated for one week with PGG at 1:1 molar ratio. Addition of CB[7] to this sample at a 1:1:5 (B) or at a 1:1:10 (C) A$\beta_{25\text{-}35}$:PGG:CB[7] molar ratio and then further incubation for two days was applied before the TEM analyzes. The exposure of pre-formed A$\beta_{25\text{-}35}$:PGG fibers to CB[7] qualitatively reduced the number of A$\beta_{25\text{-}35}$ fibers, and the most of the remaining fibers exhibited some degree of irregularity, with regions that were thicker and heavily stained.

References

(1) Wyttenbach, T., Kemper, P. R., and Bowers, M. T. (2001) Design of a new electrospray ion mobility mass spectrometer. *Int. J. Mass Spectrom. 212*, 13-23.

(2) Wyttenbach, T., Gidden, J., and Bowers, M. T. In *Ion Mobility Spectrometry - Mass Spectrometry*; Wilkins, C. L., Trimpin, S., Eds.; CRC Press: Boca Raton, FL, 2011, p 3-30.

(3) Mason, E. A. *Transport Properties of Ions in Gases*; 99 ed.; John Wiley & Sons, 1988.

(4) Gidden, J., Ferzoco, A., Baker, E. S., and Bowers, M. T. (2004) Duplex formation and the onset of helicity in poly d(CG)n oligonucleotides in a solvent-free environment. *J. Am. Chem. Soc. 126*, 15132-15140.

(5) Kim, J., Jung, I. S., Kim, S. Y., Lee, E., Kang, J. K., Sakamoto, S., Yamaguchi, K., and Kim, K. (2000) New cucurbituril homologues: syntheses, isolation, characterization, and X-ray crystal structures of cucurbit[n]uril (n=5, 7, and 8). *J. Am. Chem. Soc. 122*, 540-541.

(6) Hanwell, M. D., Curtis, D. E., Lonie, D. C., Vandermeersch, T., Zurek, E., and Hutchison, G. R. (2012) Avogadro: an advanced semantic chemical editor, visualization, and analysis platform. *J. Cheminform. 4*.

(7) Vanquelef, E., Simon, S., Marquant, G., Garcia, E., Klimerak, G., Delepine, J. C., Cieplak, P., and Dupradeau, F. Y. (2011) R.E.D. Server: a web service for deriving RESP and ESP charges and building force field libraries for new molecules and molecular fragments. *Nucleic Acids Res. 39*, W511-517.

(8) Dupradeau, F. Y., Pigache, A., Zaffran, T., Savineau, C., Lelong, R., Grivel, N., Lelong, D., Rosanski, W., and Cieplak, P. (2010) The R.E.D. tools: advances in RESP and ESP charge derivation and force field library building. *Phys. Chem. Chem. Phys. 12*, 7821-7839.

(9) Bayly, C. I., Cieplak, P., Cornell, W. D., and Kollman, P. A. (1993) A well-behaved electrostatic potential based method using charge restraints for deriving atomic charges - the RESP model. *J. Phys. Chem. 97*, 10269-10280.

(10) Frisch, M. J., Trucks, G. W., Schlegel, H. B., Scuseria, G. E., Robb, M. A., Cheeseman, J. R., J. A. Montgomery, J., Vreven, T., Kudin, K. N., J. C. Burant, J. M. M., Iyengar, S. S., J. Tomasi, V. B.*et al.*; Gaussian, Inc.: Wallingford CT, 2004.

(11) Case, D. A., Darden, T. A., T.E. Cheatham, I., Simmerling, C. L., Wang, J., Duke, R. E., Luo, R., Walker, R. C., Zhang, W., Merz, K. M., Roberts, B., Wang, B.*et al. AMBER 12*; University of California: San Francisco, 2012.

(12) Wang, J. M., Wolf, R. M., Caldwell, J. W., Kollman, P. A., and Case, D. A. (2004) Development and testing of a general amber force field. *J. Comp. Chem. 25*, 1157-1174.

(13) Humphrey, W., Dalke, A., and Schulten, K. (1996) VMD: Visual molecular dynamics. *J. Mol. Graph. Model. 14*, 33-38.

(14) Shvartsburg, A. A., and Jarrold, M. F. (1996) An exact hard-spheres scattering model for the mobilities of polyatomic ions. *Chem. Phys. Lett. 261*, 86-91.

(15) Mesleh, M. F., Hunter, J. M., Shvartsburg, A. A., Schatz, G. C., and Jarrold, M. F. (1996) Structural information from ion mobility measurements: effects of the long range potential. *J. Phys. Chem. A 100*, 16082-16086.

(16) Bleiholder, C., Contreras, S., Do, T. D., and Bowers, M. T. (2013) A novel projection approximation algorithm for the fast and accurate computation of molecular collision cross sections (II). Parameterization and application to biomolecules. *Int. J. Mass Spectrom. 345-347*, 89-96.

(17) Bleiholder, C., Wyttenbach, T., and Bowers, M. T. (2011) A novel projection approximation algorithm for the fast and accurate computation of molecular collision cross sections (I). Method. *Int. J. Mass Spectrom. 308*, 1-10.